JOURNAL OF COMPUTATIONAL PHYSICS 63, 33–66 (1986)

An Adaptive Method of Lines with Error Control for Parabolic Equations of the Reaction–Diffusion Type

M. BIETERMAN*

Laboratory of Applied Studies, Division of Computer Research and Technology, National Institutes of Health, Bethesda, Maryland 20205

AND

I. BABUŠKA†

Institute for Physical Science and Technology, University of Maryland, College Park, Maryland 20742

Received June 12, 1984; revised March 15, 1985

A piecewise linear finite element-based method of lines is presented for the numerical solution of coupled parabolic partial differential equations which model biological and physicochemical reaction–diffusion processes in one space dimension. The vertial lines emanating from the space nodes in this method change at automatically selected times when, in order to control a norm of the space discretization error, adaptive spatial regridding occurs. The regridding algorithm is an extension of one described previously by the authors [7] and is implemented in the program FEMOL 1, which uses the LSODI package [14, 15] of Hindmarsh and Painter to integrate the ordinary differential equations in time along the vertical lines. Computational results show that the method is efficient, that a posteriori estimates of the space discretization error are accurate, and that the adaptive procedure reliably controls the space discretization error.

1. INTRODUCTION

Reaction–diffusion processes occur in many branches of biology and physical chemistry. Examples include substrate transport and consumption in the microcirculation, flame propagation in combustion, nerve conduction, and interactions of mobile populations in ecosystems. These diverse phenomena are often modeled by initial boundary value problems (IBVPs) in which the governing parabolic partial differential equations (PDEs) are nonlinear and coupled only through the rates at

* Present adress: Engineering Technology Applications Division, Boeing Computer Services, MS 9C-01, Tukwila, Washington 98188.

† Partially supported by ONR Contract 0014-77-C-0623.

0021-9991/86 $3.00

which physical components react. Such IBVPs in one space dimension are the problems considered in this paper.

Solutions of these problems may decay to steady states, oscillate in time, or evolve as localized traveling waveforms. Spatial rezoning or regridding in numerical methods for time-dependent PDEs with the latter type of solutions has become quite popular. Grid evolution is generally governed by a feedback procedure in the "physical" reference frame or by explicit mappings from "physical" to "computational" coordinates, either in an a priori manner or as part of a feedback procedure. Schemes utilizing coordinate mappings are surveyed in Thompson, Warsi, and Mastin [22].

In this paper we describe the implementation of a variation of the classical method of lines (MOL) in which the space grid is updated in a feedback (adaptive)[1] procedure. The MOL reduces an IBVP through space discretization into an initial value problem for a system of ordinary differential equations (ODEs) in time. The ODEs determine spatial parameters of the solution on vertical lines extending in time. The method described here is based on a finite element formulation using linear elements in space. We refer to this approach as the FEMOL. The ODEs in the FEMOL determine nodal values of the solution. They are integrated via variable-order, variable-step implicit formulas as implemented in the LSODI package of Hindmarsh and Painter (cf. [14, 15]). In the adaptive FEMOL grids change discontinuously in time, as nodes are both added and deleted. Such regridding is often said to be locally "static," in contrast to "dynamic" regridding, where changes occur continuously in time.

Most methods described in the literature which employ static, dynamic, or combinations of both types of regridding can be viewed as MOL extensions or variations. In Miller and Miller [16], Gelinas, Doss, and Miller [12], and Miller [17], the moving finite element method was developed, where a fixed number of nodes are used and nodal positions are computed together with the solution values at the nodes. The concept of moving (in time) meshes was also used in Davis and Flaherty [12] and Flaherty *et al.* [10]. Many regridding methods for time-dependent PDEs have attractive properties. The reader is especially referred to Berger and Oliger [4], Dwyer, Kee, and Sanders [9], Gannon [11], and Harten and Hyman [13].

While these methods incorporate various principles and constraints in feedback approaches, all have similar objectives. Regridding is expected to yield high accuracy, reliability, and robustness per computational cost. It is difficult to quantitatively compare various feedback (adaptive) methods, despite the fact their goals are related, but it should be possible to measure the success or failure of each in achieving its goals. Unfortunately, the goals often are not well formulated, quantified, or used in supporting computational experiments.

[1] The terms "adaptive" and "feedback" are used interchangeably to describe numerical methods here. For analyses which distinguish between the two, see Rheinboldt [20] and Babuška and Vogelius [1].

The primary goal of the adaptive FEMOL is to control the space discretization error of the approximate solution as measured in a weighted L_2 gradient norm (weighted H^1 norm). This norm arises naturally in connection with the finite element formulation. Error control is achieved through control of computed error estimates. The a posteriori estimator used here is similar to that analyzed for linear parabolic PDEs by the authors in [6, 7]. The estimator is obtained by summing local error indicators. These are formed from PDE residuals evaluated with the approximate solution inside each of the elements.

The regridding strategy described here extends an earlier version of the authors [7] and was summarized for linear PDEs in Bieterman [5]. A grid is retained until the estimated error exceeds a preset tolerance. The error is lowered below this tolerance by adding and deleting nodes. The most important part of grid construction is a pattern recognition procedure used to determine the "shape" of the grid. In this procedure information is extracted fom the local error indicators, reduced to a grid-independent form, and relevant features taken from this reduced data are compared.

This paper is organizied as follows. Section 2 contains mathematical details of the problem and classical version of the method. The salient features of the adaptive FEMOL are described in Section 3, along with the goals of the method and the basic strategy used to achieve them. Achievement of the goals depends first and foremost on the quality of the error estimator. The estimator and the local indicators used to form it are the subjects of Section 4. In Section 5 we introduce the notion of "shape" and "intensity" to describe a grid. The specific strategy used to construct a grid is to somewhat directly control these two grid properties. This strategy and details of the refinement–derefinement algorithm are given in Section 5. In Section 6 we describe the selection of the parameter which controls grid intensity. The pattern recognition procedure used to select the function controlling grid shape is presented in Section 7. Section 8 contains the results of many carefully conducted computational experiments with four reaction–diffusion problems. These results enable one to quantitatively evaluate the performance of the method. They show how the regridding strategy is carried out, how the error estimator works, and the dependence of error control on error estimation. The final section summarizes many of the important aspects of the method.

2. Problem and Classical Method Description

Let $\Omega = \{x: -\infty < \partial\Omega^- < x < \partial\Omega^+ < \infty\}$, $\partial\Omega = \partial\Omega^- \cup \partial\Omega^+$ and $\bar{\Omega} = \Omega \cup \partial\Omega$. We are interested in finding $u = \{u^i(t, x)\}_{i=1,\text{NPDE}}$ for $t \in [0, T]$ and $x \in \bar{\Omega}$ which satisfies the differential equations

$$u_t^i - (a^i(x)u_x^i)_x = f^i(t, x, u); \qquad x \in \Omega,\ t \in (0, T],\ i = 1, \text{NPDE}, \tag{1.a}$$

the boundary conditions

$$\alpha^i(x)u^i + \beta^i(x)u_x^i = g^i(t, x); \qquad x \in \partial\Omega,\ t \in (0, T],\ i = 1, \text{NPDE}, \tag{1.b}$$

and the initial conditions

$$u^i = u_0^i(x); \qquad x \in \Omega,\ t = 0,\ i = 1,\ \text{NPDE}. \tag{1.c}$$

For $x \in \bar{\Omega}$ it is assumed that $a^i(x) \geqslant 0$, $i = 1$, NPDE, with $a^i(x) \geqslant a_0 > 0$ for at least one index i. The functions α^i and β^i determine the type of boundary conditions (BCs). It is assumed that $\beta^i(\partial\Omega^-) \leqslant 0$, $\beta^i(\partial\Omega^+) \geqslant 0$, and $\alpha^i(x) \geqslant 0$ for $x \in \partial\Omega$ and $i = 1$, NPDE. With reasonable problem data, the solution u of Eqs. (1) exists and is a smooth mapping of $[0, T]$ into the Hilbert space

$$\mathscr{H} = \{v = \{v^i\}_{i=1,\text{NPDE}} : v^i,\ v_x^i \in L_2(\Omega);\ i = 1,\ \text{NPDE}\}.$$

Here, $L_2(\Omega)$ denotes the usual space of square integrable functions on Ω, with norm and inner product $\|\cdot\|_0$ and $\langle \cdot, \cdot \rangle$, respectively. Provided approriate conditions on $\{a^i, \alpha^i, \beta^i\}_{i=1,\text{NPDE}}$ hold, the semi-norm

$$|||v||| \equiv \left\{ \sum_{i=1}^{\text{NPDE}} \langle a^i v_x^i, v_x^i \rangle \right\}^{1/2}$$

is a norm on $\mathscr{H}$.

We will denote by

$$\delta = \{\partial\Omega^- = x_0 < x_1 < x_2 < \cdots < x_{N-1} < x_N = \partial\Omega^+\} \tag{2}$$

a space grid, with nodes $\{x_n\}$ and elements $\{(x_{n-1}, x_n)\}$, and write

$$h_n = x_n - x_{n-1} \qquad \text{for} \quad n = 1,\ N. \tag{3}$$

$S(\delta) \subset \mathscr{H}$ denotes the finite element subspace of functions which are linear on each element of δ.

The *classical* version of the FEMOL is formulated in the present setting as follows. With given δ, the semi-discrete approximation $\tilde{U}$: $[0, T] \to S(\delta)$ of u satisfies the equations

$$\langle \tilde{U}_t^i(t, \cdot), \Phi^i \rangle + \langle a^i \tilde{U}_x^i(t, \cdot), \Phi_x^i \rangle + a^i(x) \frac{\alpha^i(x)}{\beta^i(x)} \tilde{U}^i(t, x)\, \Phi^i(x) \Big|_{\partial\Omega^-}^{\partial\Omega^+}$$

$$= \langle F^i(t, \cdot, \tilde{U}), \Phi^i \rangle + \frac{a^i(x)}{\beta^i(x)} g^i(t, x)\, \Phi^i(x) \Big|_{\partial\Omega^-}^{\partial\Omega^+}; \qquad t \in (0, T),\ i = 1,\ \text{NPDE},$$

$$\Phi = \{\Phi^j\}_{j=1,\text{NPDE}} \in S(\delta) \tag{4.a}$$

and

$$\tilde{U}(0, \cdot) = U(0, \cdot). \tag{4.b}$$

$U(0, \cdot) \in S(\delta)$ is the linear interpolate of $u_0(\cdot)$ and $F(t, \cdot, \tilde{U}) \in S(\delta)$ interpolates $f(t, \cdot, \tilde{U})$. Here it has been assumed for simplicity that $\beta^i(x) \neq 0$ for all i. Otherwise, $S(\delta)$ and Eqs. (4) are modified by usual finite element techniques.

Equations (4) are equivalent to requiring that the vector $\tilde{U}[t] = \{\tilde{U}^i(t, x_n)\}_{i=1,\text{NPDE};n=0,N}$ satisfies the ODEs

$$M \cdot \frac{d}{dt}\tilde{U}[t] + A \cdot \tilde{U}[t] = M \cdot F[t, \tilde{U}] + B[t]; \qquad t \in (0, T], \tag{5.a}$$

and initial condition

$$\tilde{U}[0] = U[0]. \tag{5.b}$$

In Eqs. (5), $U[0]$ and $F[t, \tilde{U}]$ are the NPDE $\cdot (N+1)$-dimensional vectors of nodal values of $U(0, \cdot)$ and $F(t, \cdot, \tilde{U})$. M and A are symmetric matrices which are positive definite and nonnegative, respectively. With an appropriate ordering of the nodal values, these matrices and the product of M and the Jacobian of $F[t, \tilde{U}]$ with respect to $\tilde{U}[\cdot]$ have half bandwidths $2 \cdot \text{NPDE} - 1$ (i.e., at most $4 \cdot \text{NPDE} - 1$ nonzero entries per row). The vector $B[t]$ has at most $2 \cdot \text{NPDE}$ nonzero entries which correspond to the values

$$\left.\{a^i(x_n)\, g^i(t, x_n)/\beta^i(x_n)\}\right\}_{\substack{i=1,\text{NPDE} \\ n=0 \text{ and } N}}.$$

Recall that $\beta^i \neq 0$ was assumed. If $\beta^i(x_0) = 0$ and $\alpha^i(x_0) \neq 0$ (Dirichlet BC), for example, this condition is implemented by modifying entries of M, A, and $B[t]$ to obtain the equations

$$\alpha^i(x_0)\frac{d}{dt}\tilde{U}^i(t, x_0) = \frac{d}{dt}g^i(t, x_0); \qquad t > 0 \text{ and } \tilde{U}^i(0, x_0) = U^i(0, x_0).$$

The FEMOL approximate solution $U(\cdot, \cdot)$ is obtained by numerically solving Eqs. (5). This is accomplished with the "stiff" implicit backward differentiation formulas in the LSODI package of Hindmarsh and Painter (cf. [14, 15]). LSODI takes an input time discretization error tolerance $\text{TOL} > 0$, advances with internally chosen time steps and integration orders, and returns $U[t]$, the approximate solution of Eqs. (5) and the vector of nodal values of $U(t, \cdot)$.

We modified the form of the local time error (per step) estimator in LSODI so that an attempt is made to obtain

$$\sum_{i=1}^{\text{NPDE}} \|\text{est}^i(t, \cdot)\|_0^2 \leqslant (\text{TOL})^2 \left(\sum_{i=1}^{\text{NPDE}} \|U^i(t, \cdot)\|_0^2 + 1 \right). \tag{6}$$

Here, $\text{est}(t, \cdot) = \{\text{est}^i(t, \cdot)\}_{i=1,\text{NPDE}} \in S(\delta)$ is the function whose nodal values are the local time error estimates computed in LSODI.

The character of the ODE initial value problem (5) is assumed to be such that

$$\sum_{i=1}^{\text{NPDE}} \|\tilde{U}^i(t, \cdot) - U^i(t, \cdot)\|_0^2 \leqslant C(\text{TOL})^2 \left(\sum_{i=1}^{\text{NPDE}} \|\tilde{U}^i(t, \cdot)\|_0^2 + 1 \right) \tag{7}$$

with a reasonable constant C independent of δ. Moreover, TOL is assumed to be selected such that $|||\tilde{U} - U|||$ is small with respect to $|||u - \tilde{U}|||$, and hence the total error $e = u - U$ satisfies

$$|||e||| \doteq |||u - \tilde{U}||| = O(\max_n h_n) \qquad \text{as} \quad \max_n h_n \to 0. \tag{8}$$

The question of how small TOL must be is not addressed here. For some results in this direction see Babuška and Luskin [2].

3. The Adaptive Femol

The MOL variation presented here differs from the MOL just described in two basic ways. First, reliable error information is obtained during problem integration by computing an a posteriori estimate $\mathscr{E}(t)$ of $|||e(t, \cdot)|||$ at each t in a set of initially provided, equally spaced times $\{t_k\}_{k=1,K} \subset (0, T)$. $\mathscr{E}$ is described in the next section. Second, adaptive regridding occurs at times $\{T_m\}_{m \geq 1} \subset \{t_k\}_{k=1,K}$. The selection of the regridding times depends on the computed values of $\mathscr{E}(\cdot)$.

Integration begins and procedes as in the nonadaptive FEMOL until regridding occurs at some time t_k. A new grid δ^+ is created from the present grid δ at t_k by uniformly subdividing some elements and removing groups of contiguous nodes to coalesce others. New initial data $U(t_k^+, \cdot) \in S(\delta^+)$ is determined simply by interpolating the already computed $U(t_k, \cdot) \in S(\delta)$ (for the present class of problems, linear interpolation is more efficient and has been observed to be no less accurate than L_2 or other "global" projections).

The grid δ^+ and data $U(t_k^+, \cdot)$ define a semidiscrete approximate $\tilde{U}(t, \cdot) \in S(\delta^+)$ for $t \geq t_k$ as in Eqs. (4) and an ODE initial value problem of the form (5) for solution values at the nodes of δ^+. Integration of this problem commences at time t_k by *restarting* LSODI with the same error tolerance TOL. ODE integration procedes smoothly through times when regridding does not occur. It continues forward in time until regridding again occurs or the final time T is reached.

Let us summarize the input and output for this procedure. The *input* provided at the initial time $T_0 = 0$ consists of

(i) a grid δ_0,

(ii) a time discretization error tolerance TOL > 0,

(iii) a space discretization error tolerance EPS > 0, and

(iv) the times $\{t_k\}_{k=1,K} = \{kT/K\}_{k=1,K}$ at wich $\mathscr{E}(\cdot)$ is computed.

The *output* from the procedure consists of

(a) spatial accuracy estimates $\{\mathscr{E}(t_k)\}_{k=1,K}$,

(b) regridding times $\{T_m\}_{m \geq 1} \subset \{t_k\}_{k=1,K}$,

(c) corresponding grids $\{\delta_m\}_{m\geq 1}$, and

(d) an approximate solution U, which is in $S(\delta_m)$ for $t\in[T_m, T_{m+1})$. (10)

There typically are a great many ODE integration time steps taken on each (t_k, t_{k+1}), and many of these intervals in each (T_m, T_{m+1}). The TOL-dependent ODE time stepsize sequence generated by LSODI generally increases on each (T_m, T_{m+1}), and it increases most rapidly just after being restarted at T_m, when LSODI is permitted to choose the initial stepsize. As in the nonadaptive FEMOL, we assume that the errors due to the grids $\{\delta_m\}_{m\geq 1}$ dominate those due to time discretization.

The *primary goal* in selecting $\{T_m\}_{m\geq 1}$ and constructing $\{\delta_m\}_{m\geq 1}$ is to obtain a reliable solution in the sense that

$$|||\, e(t,\cdot)\,||| \leq \mathrm{EPS}\,|||\, u(t,\cdot)\,|||, \qquad t\in(0, T). \tag{11}$$

The *secondary goal* is that $\{T_m\}$ and $\{\delta_m\}$ should be chosen so that

> the total work required to integrate the IBVP on $\Omega\times(0, T)$ is less than that required with the same input and any other selections of regridding times $\{T_s\}_{s\geq 1}\subset\{t_k\}_{k=1,K}$ and grids $\{\delta_s\}_{s\geq 1}$ which yield (11). (12)

The *basic strategy* used to achieve these goals is summarized as follows:

(i) Integration procedes only in the positive time direction and no information is obtained from the future.

(ii) Information is collected only at the input times $\{t_k\}$. The amount of information stored at any time is small and is discarded after one regridding takes place in the future.

(iii) Regridding occurs at some t_k if, and only if $\mathscr{E}(t_k) > 0.95\ \mathrm{EPS}|||\, U(t_k,\cdot)\,|||$.

(iv) Regridding is carried out at t_k in order that $\mathscr{E}(t_k^+) \doteq \mathrm{EPSDN}|||\, U(t_k,\cdot)\,|||$, where $\mathrm{EPSDN}\in[0.6\ \mathrm{EPS}, 0.9\ \mathrm{EPS}]$ is adaptively chosen and $\mathscr{E}(t_k^+)$ is a prediction (described in the next section) of the $|||\cdot|||$-error immediately after time t_k with the new grid.

Pure relative $|||\cdot|||$-error control is used so that the reader can better compare the ability of the method to estimate and control errors in the four problems of Section 8. In practice, EPS might better be a combined relative–absolute error tolerance, as the time discretization error tolerance TOL is here. Note that the constant 0.95 in (iii) introduces a high risk of violating (11) on some time interval (t_k, t_{k+1}). This constant was chosen in order to show the dependence of error control on error estimation in the experiments described in Section 8.

From (iii) and (iv) one sees that the regridding times are implicitly determined by EPSDN and the constructed grids. A grid is retained until $\mathscr{E}/|||\, U\,|||$ has grown to at least G times its value just after grid construction, where $G = 0.95\ \mathrm{EPS}/\mathrm{EPSDN}\in(1.05, 1.60)$. Let us remark that the character of the PDEs is assumed to be sufficiently dissipative so that the influence of local errors decreases in time.

In attempting to achieve the secondary goal (12), a work expression is employed which utilizes ODE time stepsize information and computed values of $\mathscr{E}(\cdot)$. This expression is used to select EPSDN and is described in Section 6.

4. Error Estimation

Let t be one of the given input times $\{t_k\}_{k=1,K}$ and δ of the form (2), (3) be the last space grid constructed before time t. The a posteriori estimate $\mathscr{E}(t)$ of $|||e(t,\cdot)||| = |||u(t,\cdot) - U(t,\cdot)|||$ is

$$\mathscr{E}(t) = \left\{ \sum_{n=1}^{N} \sum_{i=1}^{\mathrm{NPDE}} |\eta_n^i(t)|^2 \right\}^{1/2}, \tag{13}$$

where η_n^i is the local error indicator for the ith PDE on the nth element:

$$|\eta_n^i(t)|^2 \equiv \begin{cases} 0 & \text{if } a^i\left(\dfrac{x_{n-1}+x_n}{2}\right) = 0, \\ \dfrac{h_n^2}{12a^i((x_{n-1}+x_n)/2)} \displaystyle\int_{x_{n-1}}^{x_n} |r^i(t,x)|^2\,dx & \text{otherwise.} \end{cases} \tag{14}$$

The function $r^i(t,\cdot)$ is the residual of the ith PDE (neglecting the discontinuities at the nodes):

$$r^i(t,x) = U_t^i(t,x) - a_x^i(x)\,U_x^i(t,x) - f^i(t,x,U(t,x)). \tag{15}$$

The residual is obtained via nodal values in $U[t]$ and $(d/dt)\,U[t]$ from LSODI and integrated in (14) with 2-point Gaussian quadrature.

The quality of the estimator $\mathscr{E}$ can be measured with the *effectivity index*

$$\Theta(t) \equiv \mathscr{E}(t)/|||e(t,\cdot)|||. \tag{16}$$

This quality was theoretically analyzed in the setting of linear uncoupled PDEs by the authors [6, 7], where it was shown that

$$\max_t |\Theta(t) - 1| \to 0 \tag{17}$$

as the space grid sizes converge to zero. The key assumptions used in the proof of (17) were that the exact solution u is sufficiently smooth, u_{xx} does not degenerate to the zero function, ODE integrations are sufficiently accurate, and that the grids are not too irregular or modified too frequently.

All theoretical details have not been carried out for nonlinear reaction–diffusion systems, but computational experience suggests that similar theory applies here. The evaluation of $\mathscr{E}$ is included in many experiments in Section 8.

Let us now assume that $t \in \{T_m\}_{m \geq 1}$ and the grid δ is about to be modified. The $|||\cdot|||$-error immediately following a *proposed* regridding

$$\delta^+ = \{\partial\Omega^- = x_0^- < x_1^+ < \cdots < x_{N^+}^+ = \partial\Omega^+\}$$

is estimated with

$$\mathscr{E}(t^+) = \left\{ \sum_{j=1}^{N^+} \sum_{i=1}^{\text{NPDE}} |\eta_j^i(t^+)|^2 \right\}^{1/2}, \tag{18}$$

where $\{\eta_j^i(t^+)\}$ are predicted values of the error indicators for the grid δ^+. These indicators are determined from the already computed $\{\eta_n^i(t)\}$ in the following way.

If some element (x_{n-1}, x_n) is to be refined into the union

$$\bigcup_{j=j_0}^{j_0-1+q} (x_{j-1}^+, x_j^+)$$

of q uniform subelements, then a q-fold *decrease* in the contribution to the $|||\cdot|||$-error on (x_{n-1}, x_n) is predicted:

$$\sum_{j=j_0}^{j_0-1+q} \sum_{i=1}^{\text{NPDE}} |\eta_j^i(t^+)|^2 \equiv q^{-2} \sum_{i=1}^{\text{NPDE}} |\eta_n^i(t)|^2. \tag{19}$$

Alternatively, if some q contiguous elements $\{(x_{n-1}, x_n)\}_{n=n_0, n_0-1+q}$ in the present grid are to be coalesced to form one new element (x_{j-1}^+, x_j^+), then

$$\sum_{i=1}^{\text{NPDE}} |\eta_j^i(t^+)|^2 \equiv \left(\sum_{n=n_0}^{n_0-1+q} h_n \right)^2 \cdot \sum_{n=n_0}^{n_0-1+q} h_n^{-2} \sum_{i=1}^{\text{NPDE}} |\eta_n^i(t)|^2. \tag{20}$$

If it happens that $h_{n_0} = \cdots = h_{n_0-1+q}$, then (20) corresponds to a predicted q-fold *increase* in the contribution to the $|||\cdot|||$-error on $(x_{n_0-1}, x_{n_0-1+q}) = (x_{j-1}^+, x_j^+)$.

These predictions, as those used in [7], are based on the expectation that for $n = 1, N$

$$\sum_{i=1}^{\text{NPDE}} |\eta_n^i(t)|^2 = \frac{h_n^2}{12} \int_{x_{n-1}}^{x_n} \sum_{i=1}^{\text{NPDE}} a^i(x) |u_{xx}^i(t, x)|^2 \, dx \cdot (1 + o(h_n)) \qquad \text{as} \quad h_n \to 0. \tag{21}$$

When the grid δ is to be modified, additional information is extracted from the error indicators $\{\eta_n^i(t)\}$. A piecewise constant function is constructed:

$$w(t, x) \equiv h_n^{-1} \left(12 \sum_{i=1}^{\text{NPDE}} |\eta_n^i(t)|^2 \right)^{1/3}; \qquad x \in (x_{n-1}, x_n), \, n = 1, N, \tag{22}$$

which is an approximation of the cube root of the integrand in (21). From the definition (13) of $\mathscr{E}(t)$, one sees that

$$\mathscr{E}^2(t) = \sum_{n=1}^{N} \frac{h_n^2}{12} \int_{x_{n-1}}^{x_n} w^3(t, x)\, dx. \tag{23}$$

The function $w(t, \cdot)$ and (23) are explicitly used in determining the "shape" of the new grid δ^+.

5. Grid Shape and Intensity

In refining and derefining a grid δ, two properties of δ are changed: its shape and its intensity. To explain what is meant, we begin more generally by defining the *shape* of a positive integrable function ξ on Ω as the graph of the function

$$\mathscr{R}(x, y) \equiv \xi(x)/\xi(y); \qquad x, y \in \Omega$$

and the *intensity* of ξ simply as

$$\mathscr{I} \equiv \int_{\Omega} \xi(x)\, dx.$$

Two positive functions have identical shape if and only if they are constant multiples of one another. A positive integrable ξ can be magnified (multiplied by a constant) to get a function having any positive intensity and the shape of ξ.

The *shape* and *intensity* of a grid δ are taken to be those of the associated *grid function*

$$\xi_\delta(x) \equiv \begin{cases} 1/h_n;\ x \in (x_{n-1}, x_n) & \text{for } n = 1, N, \\ 0.5(1/h_n + 1/h_{n+1});\ x = x_n & \text{for } n = 1, N-1. \end{cases} \tag{24}$$

It is easily checked that δ has intensity $\mathscr{I}_\delta = N$.

Let us briefly examine the effects of grid shape and intensity on the estimated $|||\cdot|||$-error in the present method. To this end, at a time t when a grid δ is being used, we may use ξ_δ in the expression (23) for $\mathscr{E}^2(t)$ to obtain

$$\begin{aligned} \mathscr{E}(t) &= \Lambda(w(t, \cdot), \xi_\delta) \\ &\equiv \left(\frac{1}{12} \int_{\Omega} \frac{w^3(t, x)}{\xi_\delta^2(x)}\, dx \right)^{1/2}. \end{aligned} \tag{25}$$

Since $w(t, \cdot)$ (cf. (22)) tends toward a grid-independent function as the information defining it improves, let us consider it to be known.

Now, had each element of δ been bisected at the creation of the grid, for example, the resulting grid would have had the same shape and twice the intensity of δ. One

sees by examining the integrand in (25) that $\mathscr{E}(t)$ would have been half as large. Alternatively, if the $N-1$ interior nodes of δ had been rearranged (i.e., the same number of extra nodes added as deleted here) then the shape of δ would have been different, but the intensity would not. The change in $\mathscr{E}(t)$ then would have depended strongly on how the shape of δ had changed with respect to the shape of $w(t, \cdot)$.

In constructing a grid, *all* reasonable refinement/derefinement algorithms for time-dependent PDEs must select a shape and an intensity for the grid which will work in the future. This is usually done indirectly: by focussing completely on local error estimates, for example. In the adaptive FEMOL, these two properties are controlled more directly. A grid is constructed by

(i) explicitly selecting a positive *model grid function* ξ,

(ii) magnifying ξ to yield an implicitly defined *model grid intensity* $\mathscr{I}$, and

(iii) refining and derefining so that the resulting grid has a shape closely resembling that of ξ, with the number of elements approximately equal to $\mathscr{I}$.

Let T_m be the time at which a grid δ^+ is to be constructed from δ. Recalling the *basic* regridding strategy described in Section 3, we know that

$$\frac{\mathscr{E}(T_m)}{\|\!| U(T_m, \cdot) |\!\|} > 0.95 \text{ EPS}$$

and that the predicted error immediately following time T_m with δ^+ is to satisfy

$$\frac{\mathscr{E}(T_m^+)}{\|\!| U(T_m, \cdot) |\!\|} \doteq \text{EPSDN}, \tag{26}$$

with EPSDN $\in$ [0.6 EPS, 0.9 EPS] still to be chosen. The model intensity $\mathscr{I}$ is defined by (26). $\mathscr{I}$ is the minimum intensity that δ^+ can have while having the shape of ξ and yielding (26).

Assume that ξ and EPSDN have already been selected. The construction of δ^+ is then carried out as follows. The elements $\{(x_{n-1}, x_n)\}_{n=1,N}$ of δ are *uniformly subdivided* or *coalesced* according to desired new local element sizes at the midpoints $\{x_{n-1/2}\} = \{(x_{n-1} + x_n)/2\}$ of δ:

$$h^+(x_{n-1/2}) \equiv \frac{1}{C \cdot \xi(x_{n-1/2})}; \qquad n = 1, N. \tag{27}$$

The constant $C > 0$ in (27) is initialized in a predetermined way and is iteratively adjusted until (26) holds. More specifically, C is initialized as

$$C_0 = \frac{\Lambda(w(T_m, \cdot), \xi)}{\text{EPSDN} \, \|\!| U(T_m, \cdot) |\!\|}$$

and nonnegative "refinement" integers $\{\mathrm{MOD}(n)\}_{n=1,N}$ are obtained from the integral parts of the "ratios" $\{h_n/h^+(x_{n-1/2})\}_{n=1,N}$ of old to desired new element sizes. An element is marked for uniform subdivision into MOD elements if its MOD value exceeds one; it is marked for retention of MOD = 1; and a group of contiguous old elements are marked for coalescence into one new element if their MOD values are zero and their element "ratios" sum approximately to one.

Using $\{\mathrm{MOD}(n)\}_{n=1,N}$ and the already computed local error indicators $\{\eta_n^i(T_m)\}$ for δ, $\mathscr{E}(T_m^+)$ is obtained as described in Section 4, allowing the computation of

$$F = F(C_0) = \frac{\mathscr{E}(T_m^+)}{\mathrm{EPSDN}\,|||\,U(T_m, \cdot)\,|||} - 1.$$

The iteration terminates if $F(C_0)$ is "close" to zero. Otherwise, F is assumed to have a zero bracketed by 0 and C_0 if $F(C_0) < 0$ and by C_0 and $C_0(1 + 2F(C_0))$ if $F(C_0) > 0$, and bisection is used to iteratively adjust C and obtain a new grid.

Further details of this grid construction algorithm are not given here, but several points are noted. While some mesh constraints are incorporated naturally throught the selection of ξ, none of the usual mesh constraints (on element subdivision ratios, ratio of neighboring element sizes, number of contiguous elements coalesced, etc.) are explicitly imposed in the above algorithm. The algorithm is relatively successful in controlling $\mathscr{E}(T_m^+)$ with a small number of iterations. This is primarily due to the good starting value for C which improves as EPS (and EPSDN) decreases and the number of elements used in each grid increases. With EPS in the range (0.02, 0.20), as was used in the experiments described in Section 8, typical final values of $|F(C)|$ and number of iterations per grid were 0.03–0.09 and 3–8, respectively.

In view of (27), one can expect that the grid function $\xi_{\delta^+}(\cdot)$ associated with δ^+ will resemble the function $C \cdot \xi(\cdot)$ in shape and intensity. Furthermore, one expects as in (25) that

$$\begin{aligned} \mathscr{E}(t) &\doteq \Lambda(w(t, \cdot), C\xi) \\ &= \frac{1}{C}\Lambda(w(t, \cdot), \xi); \qquad t \geqslant T_m, \end{aligned} \tag{28}$$

and from (26) that

$$\frac{1}{C}\left\{\frac{\Lambda(w(T_m, \cdot), \xi)}{|||\,U(T_m, \cdot)\,|||}\right\} \doteq \mathrm{EPSDN}. \tag{29}$$

From (28) it is clear that ξ should reflect the present and predicted future shape of $w(t, \cdot)$. ξ is chosen to be a majorant of $w(T_m, \cdot)$ in the adaptive FEMOL. The selection process anticipates the future through comparison of a small amount of information collected at T_m and the previous regridding time T_{m-1}. This process is described in Section 7.

The intensity, or number of elements in δ^+ (and number of ODEs in time to be solved) depends both on ξ and the final value of C in (27). Once ξ has been selected, however, the intensity is determined by the parameter EPSDN, as evidenced by the inverse relation between C and EPSDN in (29). The selection of EPSDN is now described.

6. Control of Grid Intensity

Assume that the model grid function ξ has been chosen at a time T_m when a grid δ^+ is to be constructed from δ. The parameter EPSDN determining the intensity of δ^+ is selected in an attempt to minimize the work per future (unknown) time step $T_{m+1} - T_m$ which will be required with a grid having the shape of ξ.

Consider two extreme values of EPSDN. If EPSDN is chosen to be 0.6 EPS (smallest permitted value), $T_{m+1} - T_m$ would be as large as possible, but so also would be the number of ODEs, since this number depends inversely on EPSDN. With EPSDN = 0.9 EPS (largest permitted value), the smallest ODE system would be integrated for the shortest period of time. The sum of such integrations could be quite costly, not only because of grid construction costs, but also since efficient use of an ODE solver whose internal stepsizes increase is made only if the solver is not frequently restarted.

If $T_m = T_1$ (first regridding), EPSDN is taken to be 0.9 EPS. Otherwise, it is selected by estimating the marginal benefit which would have resulted, had the value EPSDN_{m-1} of EPSDN used at T_{m-1} been altered. Let

$$\varepsilon(t) = \left(\frac{0.95 \text{ EPS}}{\sup_{s \in (T_{m-1}, t)} \mathscr{E}(s) / \| U(s, \cdot) \| \| \|} \right) \cdot \text{EPSDN}_{m-1}$$

for $t > T_{m-1}$. The number $\varepsilon(t)$ is an estimate of the largest value which EPSDN *could* have taken at T_{m-1} while leading to successful PDE integration (i.e., $\mathscr{E} / \| U \| \leqslant 0.95$ EPS) on (T_{m-1}, t). Note that $\varepsilon(\cdot)$ decreases on (T_{m-1}, T_m) and, by the basic regridding strategy described in Section 3, that $\varepsilon(T_{m-1}^+) \doteq 0.95$ EPS and $\varepsilon(T_m) \leqslant \text{EPSDN}_{m-1}$.

The work *per* regridding time step which *would* have been required by selecting EPSDN = $\varepsilon(t)$ at T_{m-1} can be expressed as

$$\text{WORK}(t) = \frac{(\text{STEP}(t) + \tilde{c})}{(t - T_{m-1})\, \varepsilon(t)}.$$

Here, STEP(t) is the number of ODE time steps taken on (T_{m-1}, t) with EPSDN = EPSDN_{m-1}. The constant $\tilde{c}$ is related to the overhead incurred at T_{m-1} in grid construction and data initialization.

Using stepsize information returned from the ODE solver, computed values of $\mathscr{E}(\cdot)$ and simple extrapolation for $t > T_m$, profiles of $\mathscr{E}(\cdot)$ and WORK($\cdot$) are

updated as time increases and are used to determine an "optimal" value of EPSDN at T_{m-1} in retrospect. This value then governs the selection of EPSDN at T_m. Details of the final selection are not important. What is important is that changes in EPSDN *smoothly reflect observed trends.* Here, EPSDN is increased (decreased) by no more than 0.02 EPS (0.05 EPS) from one regridding time to the next. Such relatively small changes in EPSDN can be considered as insignificant in constructing a single grid, since as partially indicated in Section 5, the relative $|||\cdot|||$-error can be controlled only to within this margin of error of being EPSDN after grid construction. It is in the *sum* of such changes in EPSDN that the observed trends have an impact on the method.

7. Control of Grid Shape

As indicated in Section 5, the shape of the grid δ^+ constructed from δ at time T_m resembles that of the model grid function ξ, which is chosen as a majorant of the function $w(T_m, \cdot)$. Recall that $w(T_m, \cdot)$ is an approximation of a function related to the exact solution's second space derivatives at T_m (cf. (22)) whose values are extracted from the local error indicators for δ. The process of selecting ξ is introduced by considering two extreme possibilities:

(i) $\xi(\cdot) = w(T_m, \cdot)$ and

(ii) $\xi(\cdot) = \max_{x \in \bar{\Omega}} w(T_m, x)$ (i.e., a constant function).

Consider ξ as in (i). Using the representation (28) for the predicted error estimate $\mathscr{E}(T_m^+)$ immediately after T_m and standard arguments of the calculus of variations, as in Babuška and Rheinboldt [3], it can be shown that the resulting grid δ^+ would have the least intensity of all grids lowering the estimated relative $|||\cdot|||$-error to any given EPSDN value. Since nothing is known for certain about the future shape of $w(t, \cdot)$ and this choice yields the ODE system of smallest possible size, one might call (i) the *low cost* alternative.

The local error indicators would be approximately equilibrated with (i), but only *near* time T_m if the shape of $w(t, \cdot)$ *rapidly* changes. Because an immediate and costly regridding could be necessitated, the choice (i) is not "optimal" in any practically useful sense of the word for parabolic PDEs whose solutions' higher derivatives undergo changes in shape. For such problems, (i) might be better termed the *high risk* alternative. The local orientation of (i) introduces a strong dependence of error control on the input parameters (i.e., the probability of a failure occurring on some interval (t_k, t_{k+1}) is high) *and* a strong dependence on *each* piece of local information (it is often the case that a "few" of the local indicators defining $w(T_m, \cdot)$ are relatively very inaccurate).

The choice (ii) of ξ represents the opposite end of the risk-cost spectrum. It is a *high cost* alternative, since the resulting grid δ^+ would be nearly uniform and have the largest intensity of all reasonable grids lowering $\mathscr{E}/|||U|||$ to any given EPSDN

value. It imposes a *low risk* of losing control over errors, since unpredictable changes in the shape of higher solution derivatives would be accounted for, as well as isolated instances of inaccurate local information.

Neither (i) nor (ii) represents a viable alternative. Heuristics must be employed to balance risk and cost and to predict the future. *All* reasonable algorithms of the present type must use heuristics to predict the future, since the future is generally far ahead of the present: much farther than for which accurate and inexpensive local extrapolations can be used.

Physical reasoning can be used (i.e., mass conservation, expected wave speeds, etc.) or numerical simulations can be adopted (i.e., global extrapolations, averaged or extended information, etc.). Can such prediction processes ever be quantitatively assessed or compared, or better justified in a general way? If so, the first step may be to see them for what they are: pattern recognition processes. Such a process consists of three (generally nondistinct) stages:

(i) *Representation.* Reduction of (perhaps "noisy") data into a convenient and invariant form.

(ii) *Feature Extraction.* Relevant measurements taken from the reduced data.

(iii) *Classification.* Decisions made by comparing feature values in an attempt to improve recognition or to avoid misrecognition.

Let us use this framework and terminology to describe the construction of ξ at time T_m. The "pattern" we wish to predict, or recognize is the shape of the function

$$\bar{w}(x) \equiv \max_{t \in [T_m,\, T_m+1]} w(t, x),$$

where T_{m+1} is *unknown*, but $T_{m+1} - T_m$ is assumed to be comparable to $T_m - T_{m-1}$. The attempt to do this consists of constructing a piecewise linear ξ which majorizes $w(T_m, \cdot)$ and whose shape approximates that of $\bar{w}$. The reasoning behind this choice comes from a variational principle *related* to the present problem and which involves the functional Λ used in the representation (28) of $\mathscr{E}$.

To construct ξ, each finite element grid is required to contain the *fixed* nodes of a uniform macro grid Δ. Δ is supplied as input at the initial time and is a 3-level grid, whose several "large" level 1 macro elements each have size $4H$, and whose level 2 and 3 subelements have sizes $2H$ and H, respectively. The size H ($4H$) is related to the *maximum* (minimum) *risk* of losing control over $|||e|||$ that one is a priori willing to take and the *minimum* (maximum) *price* one is willing to pay to keep it. The algorithm for constructing ξ tries to manage risk and cost on each level 1 macro element $(X, X+4H)$ by first

Reducing data. The many pieces of data defining $w(T_m, \cdot)$ on $(X, X+4H)$ are replaced by three piecewise constant functions $\{W_\mu(T_m, \cdot)\}_{\mu=1,2,3}$, where $W_\mu(T_m, \cdot)$ takes the maximum value of $w(T_m, \cdot)$ on each of the $2^{\mu-1}$ level μ macro elements contained in $(X, X+4H)$. In a similar manner, three piecewise con-

stant representations $\{W_\mu(T_{m-1}, \cdot)\}_{\mu=1,2,3}$ of $w(T_{m-1}, \cdot)$ on $(X, X+4H)$ were formed at time T_{m-1}, where $w(T_{m-1}, \cdot) \equiv 0$ if $T_{m-1} = 0$ (the initial time).

What relevant *features* can be *extracted* from these representations? In solving many parabolic reaction–diffusion problems, it has been observed that there often is a *correlation, on some scale*, between spatial differences in $w(T_{m-1}, \cdot)$ and the way w subsequently grows in time. The algorithm looks for such a correlation on $(X, X+4H) \times (T_{m-1}, T_m)$ by taking three measurements:

$$\mathcal{M}_\mu \equiv \int_X^{X+4H} |W_3(T_m, x) - W_\mu(T_{m-1}, x)|\, dx; \qquad \mu = 1, 2, 3.$$

These three feature values are used to *classify* the evolution of w on $(X, X+4H) \times (T_{m-1}, T_m)$. An "active" level is taken to be that corresponding to the largest index $\mu^* \in \{1, 2, 3\}$ for which

$$\mathcal{M}_{\mu^*} \leqslant \mathcal{M}_\mu; \qquad \mu = 1, 2, 3.$$

If $\mu^* = 3$ (which always is the case at the first regridding time T_1), either w did not grow on $(X, X+4H) \times (T_{m-1}, T_m)$ or it is concluded that spatial differences in w at T_{m-1} were not the source of its growth. If $\mu^* = 2$ (1), it is concluded that either a clear correlation existed on the scale $2H$ ($4H$) or w evolved in a way which was unpredictable at T_{m-1} on any smaller space scale.

Determining an "active" level μ^* for $(X, X+4H)$ can be interpreted as choosing one of three directions in the (x, t)-plane. The directions are defined by the magnitudes of time and space differences, $\{W_3(T_m, \cdot) - W_3(T_{m-1}, \cdot)\}$ and $\{W_3(T_{m-1}, \cdot) - W_\mu(T_{m-1}, \cdot)\}$ of W_3, which is the most local of the three representations of w. The direction corresponding to μ^* is that along which $W_3(t, \cdot)$ changed the least for $t \in (T_{m-1}, T_m)$.

Having classified the *past* evolution of w on each level 1 macro element in Δ, these classifications are used to *predict* the *extent* to which spatial differences in $w(T_m, \cdot)$ will affect the size of $w(t, \cdot)$ in neighboring regions for $t > T_m$. A *macro subgrid* consisting of the boundary nodes of every large level 1 element and the boundary nodes of every "active" level 2 or 3 element is formed (i.e., if $u^* = 2$ for some $(X, X+4H)$, then the node $X+2H$ is in the subgrid). The model function ξ is taken to be the *piecewise linear* function on the subgrid whose jth subgrid nodal value is equal to the maximum of $w(T_m, \cdot)$ between the $j-1$st and $j+1$st subgrid nodes. These values are obtained from those of the piecewise constant representations $\{W_\mu(T_m, \cdot)\}$, which are subsequently stored for use in computing feature values at the next regridding time.

There are two important effects of choosing ξ to be continuous and piecewise linear, as opposed to being piecewise constant. First, the dependence of the selection process on the input macro grid Δ is lessened. Second, the finite element grid δ^+ is smoothened, since the local element size $h^+(x)$ at $x \in \Omega$ is inversely proportional to $\xi(x)$.

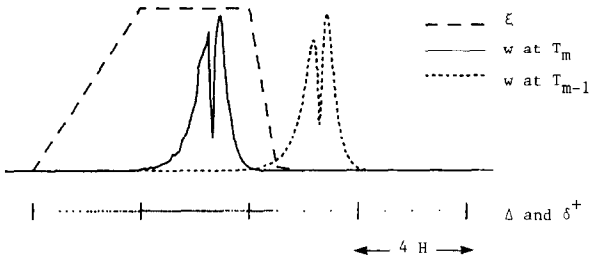

FIG. 1. Construction of ξ and grid δ^+ at time $T_m = 3.8 \times 10^{-3}$ in Example 4 of Section 8.

We show how ξ was constructed from w and how the shape of ξ determined that of the grid δ^+ in two examples taken from Section 8. In these examples, the function w was extracted from the local error indicators, as described in Section 4. The results are pictured in Figs. 1 and 2, where Δ is the 3-level macro grid whose level 1 elements are delineated by vertical hash marks.

Figure 1 depicts the model grid function ξ for Example 4, in which temperature and a single species concentration propagate in a flame front from right to left. Here, δ^+ is the grid pictured at $T_m = 3.8 \times 10^{-3}$ in Fig. 11 of Section 8.

The "active" levels in the four level 1 macro elements shown in Fig. 1 were selected to be (from left to right) 1, 1, 3, and 3. ξ localizes the right side of $w(T_m, \cdot)$ as much as possible, since w has not grown in that region. The algorithm detects a correlation between spatial differences in $w(T_{m-1}, \cdot)$ and the growth of w at the left, however, and the extension of ξ to the left shows how the movement of w is predicted.

By looking ahead of the moving front, where w is predicted to grow in the future, we see especially well how the shape of ξ determined the shape of the grid δ^+. While ξ is constant on the second level 1 macro element pictured, the corresponding nodes of δ^+ are not quite uniformly spaced, since regridding consists of refining and derefining the (not pictured) previous grid. The parameter EPSDN determining the intensity of δ^+ was chosen to be 0.85 EPS in the situation pictured in Fig. 1. Had the relative $|||\cdot|||$-error been reduced to approximately 0.6 EPS by taking EPSDN equal to this value, for example, $\frac{3}{2}$ as many nodes would have been distributed in the same relative way as pictured. The majority of the extra nodes would have been located *in* the front *at* T_m, where they never will be needed to lower the $|||\cdot|||$-error. The remaining portion placed ahead of the front would only extend the next regridding time by a small amount.

Figure 2 shows the function ξ and the grid δ^+ which were constructed in the population ecology model in Example 1 of Section 8. δ^+ is the grid pictured in Fig. 4 at $T_m = 0.6$, when the populations are in the midst of their evolution from one localized spike to a spatially oscillatory steady state with several local maxima spread over the entire domain.

The "active" levels in the 3-level macro grid Δ were selected to be 2 in the two central level 1 elements at time T_m and 1 in all others. This reflects the fact that the

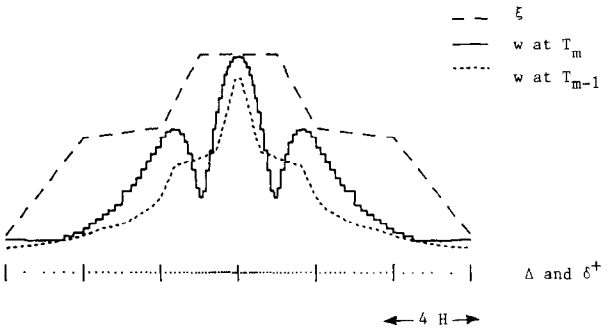

FIG. 2. Construction of ξ and grid δ^+ at time $T_m = 0.6$ in Example 1 of Section 8.

spatial *scale* on which the growth of w is correlated with differences of $w(T_{m-1}, \cdot)$ is *larger* on the sides of the domain than at the center. As in Fig. 1, we see how the shape of ξ determined the shape of δ^+. The parameter EPSDN determining the intensity of δ^+ was chosen to be 0.85 EPS at T_m, as it was in the previous example. Unlike in the the propagating flame problem, however, where EPSDN was changed very little from one regridding time to the next, EPSDN was steadily decreased in regriddings subsequent to the one pictured in Fig. 2. It becomes computationally more efficient to increase the intensities of the grids as their shapes become more constant and the spreading influence of w is predicted.

The strengths of coupling multigrid feature extraction with implicit, low order prediction in time lie in the generality of the approach, its empirical success in predicting shape, and the potential application of similar techniques in two or three space dimensions. It is not important that binary, 3-level macro girds are used. Experience indicates that the process of keeping risk and cost low through implicit shape prediction improves with p-level macro grids as p is increased, provided a reasonable number of large level 1 elements are present. It does seem important, however, that explicit shape predictors using representations of w at past regridding times not be used. The mesh sizes H and $T_m - T_{m-1}$ are *not* asymptotically small. Explicit Taylor expansions using these mesh sizes can be very inaccurate and readily destabilize the process they are meant to control.

8. COMPUTATIONAL EXPERIMENTS

The results of applying the adaptive FEMOL to numerically solve four reaction–diffusion problems are described here. These problems are of varying difficulty and were chosen to give a representative evaluation of the performance of the method.

Most of the experiments fall into one of two categories. In the first, a reasonable set of input parameters was fixed in each problem and the adaptive method was

applied with a decreasing sequence of space and time discretization error tolerances EPS and TOL, where each TOL value was small with respect to the corresponding EPS value. In the experiment in the second category, these same TOL values were used with the same method, but in which no feedback related to regridding was processed, a posteriori error estimates were only computed at few target times, and increasing numbers of uniform, time-independent finite elements were used.

The most important component of the adaptive method is the a posteriori error estimator $\mathscr{E}(t)$ (cf. Sect. 4), on which most automatically made decisions are based. The quality of $\mathscr{E}(t)$ is examined for both changing and unchanging grids with the effectivity index $\Theta(t) = \mathscr{E}(t)/|||\, e(t)\, |||$, where a very accurate approximation was used to compute the error $e = \mathbf{u} - \mathbf{U}$ when the exact solution $\mathbf{u}$ was not available. Let us recall from Section 2 that $|||\cdot|||$ is a weighted L_2 gradient norm (weighted H^1 norm), and that $|||\, e\, |||$ is predicted by theory to converge linearly to zero with decreasing local space grid sizes.

The primary goal (cf. (11), Sect. 3) of the adaptive FEMOL is to keep the relative $|||\cdot|||$-error below the tolerance EPS at all times. The method is relatively successful in achieving this objective, and we shall see that achievement of this goal depends strongly on the quality of $\mathscr{E}$. Rough estimates of the cost in controlling the error are gotten by comparing the CPU times required in the adaptive and non-adaptive runs. These times include a small amount required in I/0 associated with the experiments, but within each experiment they provide a fair estimate of the total cost.

The secondary goal (cf. (12), Sect. 3) of the adaptive FEMOL is to keep costs as low as possible, *given* a set of input and the control mechanisms of the method. Note that the CPU time comparisons mentioned above do not provide a fair measure of performance for this goal. At the end of this section we summarize results of an experiment designed to more adequately gage the relative cost of the adaptive procedure.

All experimental runs were made using the program FEMOL 1, double precision arithmetic, and the FORTRAN H compiler on the IBM System 370/3081K at the NIH. The notation used to describe the experimental results has been introduced earlier or is self-evident, with the exceptions of

$$\text{CPU} = \text{IBM 3081K sec},$$

$$\text{mean NO. ELTS.} = (1/T) \cdot \sum_{m \geqslant 1} N_{m-1}(T_m - T_{m-1}),$$

where N_{m-1} is the number of finite elements used from time T_{m-1} to time T_m, and $\Delta(J, 2J, 4J)$, which denotes a 3-level macro grid containing J, $2J$, and $4J$ level 1, 2, and 3 macro elements, with a total of $4J + 1$ fixed, uniformly spaced nodes (cf. Section 7).

Example 1. (Population Ecology Model). The system considered here was proposed by Murray [19] to model certain planktonic predator–prey situations in

which crowding is a factor. The predators v (zooplankton) and essentially static prey u (phytoplankton) satisfy

$$u_t - 0.0125\, u_{xx} = [f(u) - v]u,$$
$$v_t - v_{xx} = [u - g(v)]v, \qquad t > 0,\ x \in (0, 2.5), \tag{30}$$
$$u_x = v_x = 0, \qquad t > 0,\ x = 0, 2.5, \tag{31}$$

and

$$u = u_0, \qquad v = v_0, \qquad t = 0,\ x \in (0, 2.5), \tag{32}$$

where

$$f(u) = (35 + 16u - u^2)/9,$$
$$g(v) = (5 + 2v)/5, \tag{33}$$

and the initial populations $\{u_0, v_0\}$ are as pictured in Fig. 3, along with the steady state to which $\{u, v\}$ evolves. There are many steady state solutions of Eqs. (30), (31) (the stable solution $\{u, v\} = \{5, 10\}$ of the diffusionless ODE system, for example), and the one to which $\{u, v\}$ evolves depends on which eigenfunction of the linearized coupled elliptic operator the perturbation of the initial data from $\{5, 10\}$ most resembles. These piecewise linear initial data were represented exactly in all of the experiments described here.

This problem is relatively easy, and a *properly selected* number of uniformly spaced grid points would adequately keep the errors below a desired tolerance. The role of the adaptive FEMOL in this problem is that of a convenient and reliable tool, with which the probability of success in achieving the goal (11) in *one* application is high.

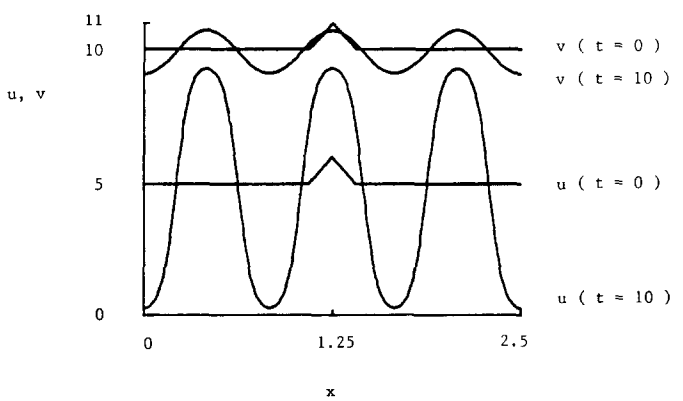

FIG. 3. Initial and steady state solutions of population ecology model in Example 1.

TABLE I

Results for Example 1 (*NONADAPTIVE*): REL ERR $= |||e|||/|||\mathbf{u}|||$ ($\mathbf{u} = \{u, v\}$) and $\Theta = \mathscr{E}/|||e|||$ Computed at $t_p = p$, $p = 1, 10$

No. elts. (unif.)	ODE TOL	REL ERR mean t_p	REL ERR max t_p	$\lvert\Theta - 1\rvert$ mean t_p	$\lvert\Theta - 1\rvert$ max t_p	CPU
32	$\tau = 10^{-3}$	0.19	0.20	0.016	0.030	1
64	$\tau/2$	0.09	0.10	0.003	0.005	2
128	$\tau/4$	0.05	0.05	—	—	6
256	$\tau/8$	0.02	0.02	—	—	21

Tables I and II summarize the results for this problem. In computing the relative $|||\cdot|||$-error and Θ at the 10 target times for the entries of these tables, the "exact" solution $\mathbf{u} = \{u, v\}$ was taken to be the numerical solution computed with 512 uniform elements and very accurate ODE time integration in the nonadaptive FEMOL. The approximations computed with the input parameters in rows 3 and 4 of these tables were too accurate to be compared with $\mathbf{u}$. The corresponding listed relative $|||\cdot|||$-errors were therefore taken to be those estimated in the method.

The value τ in Table I, row 1 was chosen as the largest value of TOL for which the maximum relative $|||\cdot|||$-error due to time discretization was less than 0.01. All other input TOL values in Tables I and II were chosen by subdividing τ, as might be done in practice. This same procedure was repeated in Examples 2 and 3.

Note the very high quality of the error estimator $\mathscr{E}$ in this example, as seen in the $|\Theta - 1|$ columns of both Tables I and II. In no instance did the estimated $|||\cdot|||$-error differ from the true $|||\cdot|||$-error by over 2.4%. This difference evidently diminishes as the relative $|||\cdot|||$ error $\to 0$, more rapidly in the uniform nonadaptive case than in the adaptive.

TABLE II

Results for Example 1 (*ADAPTIVE*): REL ERR and Θ Computed as in Table I, 32 Uniform Elements Initially, 3-Level Macro Grid $\Delta(8, 16, 32)$ Used, REL ERR Estimated and Regridding Permitted at 50 Times in (0, 10]

EPS	MESH MODS	No. elts. mean	No. elts. max	ODE TOL	REL ERR mean t_p	REL ERR max t_p	$\lvert\Theta - 1\rvert$ mean t_p	$\lvert\Theta - 1\rvert$ max t_p	CPU
$\varepsilon = 0.2$	2	40	44	$\tau = 10^{-3}$	0.17	0.18	0.021	0.034	2
$\varepsilon/2$	5	71	78	$\tau/2$	0.09	0.10	0.015	0.025	4
*$\varepsilon/4$	4	134	148	$\tau/4$	0.05	0.05	—	—	10
$\varepsilon/8$	6	290	332	$\tau/8$	0.02	0.02	—	—	43

We next observe that the adaptive FEMOL successfully achieved its primary goal in all 4 runs, as witnessed by comparing the desired maximum relative $|||\cdot|||$-errors in the EPS column of Table II with the actual maximum relative $|||\cdot|||$-errors. In doing this, the mean number of elements used in each run exceeded the corresponding number of uniform elements by 5–25%. The actual surcharge was about 100%, however, as is seen by comparing CPU times in Tables I and II. We mention that the selection of the uniform finite element grid providing a desired accuracy EPS could be expensive, and this cost is *not* reflected in the CPU entries of Table I. The adaptive method must have higher overhead costs than the non-adaptive method, since the adaptive method makes decisions during the computations and is geared to deal reliably with a large class of problems. Because this problem is so simple, the 100% surcharge is irrelevant.

The adaptive constructed grids in one of the runs are pictured in Fig. 4. The input and results for this run are summarized in the row marked with an asterisk in Table II. The construction of the grid at $t = 0.6$ was described in Section 7 and pictured in Fig. 2. We see that the nodes lead the spreading of $\{u_{xx}, v_{xx}\}$ and the local errors. The selection of these grids was "guided" with the 3-level macro grid $\Delta(8, 16, 32)$. The parameter EPSDN, allowed in all examples to vary in [0.6 EPS, 0.9 EPS], was chosen here to be no less than 0.7 EPS.

Another set of grids for this problem are pictured in Fig. 5. These grids were constructed by the adaptive FEMOL with the parameter EPSDN *fixed* as 0.9 EPS, i.e., the freedom of the method to determine the intensities of the grid (cf. Section 5) was restricted, as the relative $|||\cdot|||$-error was lowered to just under EPS in each regridding. The number of nodes used in this run was smaller than in that corresonding to Fig. 4, but the cost as measured in elapsed CPU time for this latter run was 60% higher, while the maximum relative $|||\cdot|||$-error was no lower.

Example 2. (FitzHugh–Nagumo Equations; cf. [18, 21]). The version of these equations considered here provides a conceptual model of ionic current flow across

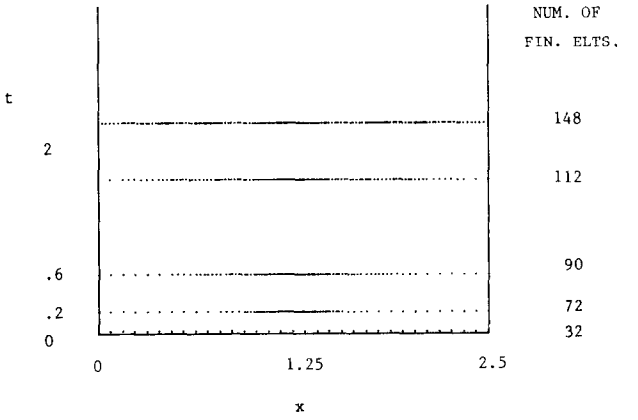

FIG. 4. Adaptively constructed grids for Example 1. Parameters as in * row of Table II.

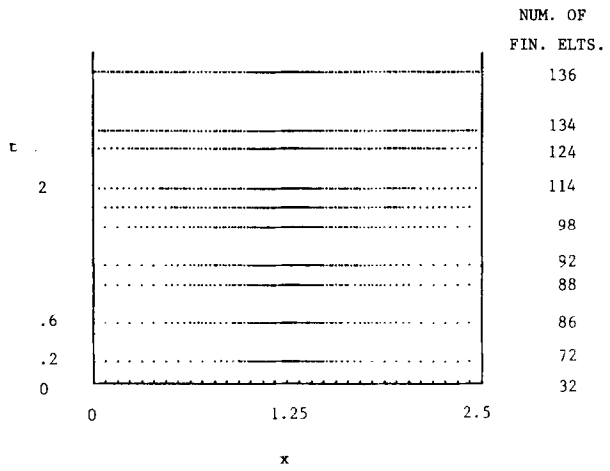

FIG. 5. Adaptively constructed grids or Example 1. Parameters as for run corresponding to Fig. 4 except that EPSDN $\equiv$ 0.9 EPS.

a semi-infinite nerve membrane. An electro-chemical potential u and "recovery" variable v satisfy

$$\begin{aligned} u_t &= u_{xx} + f(u) - v, \\ v_t &= b(u - cv), \qquad t > 0,\ x \in (0, 120), \end{aligned} \tag{34}$$

$$\begin{aligned} u_x(t, 0) &= -I/2, \\ u_x(t, 120) &= 0, \qquad t > 0, \end{aligned} \tag{35}$$

and

$$u = v = 0, \qquad t = 0,\ x \in (0, 120), \tag{36}$$

where

$$f(u) = u(u - a)(1 - u) \tag{37}$$

and here

$$\begin{aligned} a &= 0.139, \\ b &= 0.008, \\ c &= 2.54, \\ I &= 0.45. \end{aligned} \tag{38}$$

I represents the magnitude of a constant current applied at the left end of the nerve and b is the reciprocal of the time scale associated with the recovery of the nerve.

Numerical studies in Mitchell and Manoranjan [18], Rinzel [21] and elsewhere indicate the sensitivity of the solution behavior to changes in the parameters a, b, c, and I. Preliminary studies here suggest that with the values in (38), repetitive pulses (in u and v) traveling at speed $\doteq 0.4$ are generated with firing frequency $\doteq 0.77 \times 10^{-2}$. Firing frequency is defined as the reciprocal of the temporal period for a solution appearing to be a traveling wave for large x and t.

The evolution of $\mathbf{u} = \{u, v\}$ is shown in Fig. 6, where values were computed in one of the most accurate nonadaptive runs. It is noted that because of the diffusionless form of the second of Eqs. (34), only $u_x - U_x$ is explicitly controlled in the adaptive FEMOL, and the accuracy of approximating v enters naturally through its role in the residual of first of Eqs. (34).

The results for this problem are summarized in Tables III and IV. The relative $\|\cdot\|$-error and Θ were computed with the "exact" solution as obtained via 960 uniform elements and very accurate ODE time integration in the nonadaptive FEMOL. Estimated values were used for the relative errors in the most accurate entries of these tables, as was done in Example 1.

The quality of $\mathscr{E}$ is seen in the $|\Theta - 1|$ columns of Tables III and IV. At time $t = 80$, when a new pulse is rapidly developing at the left spatial boundary, the error

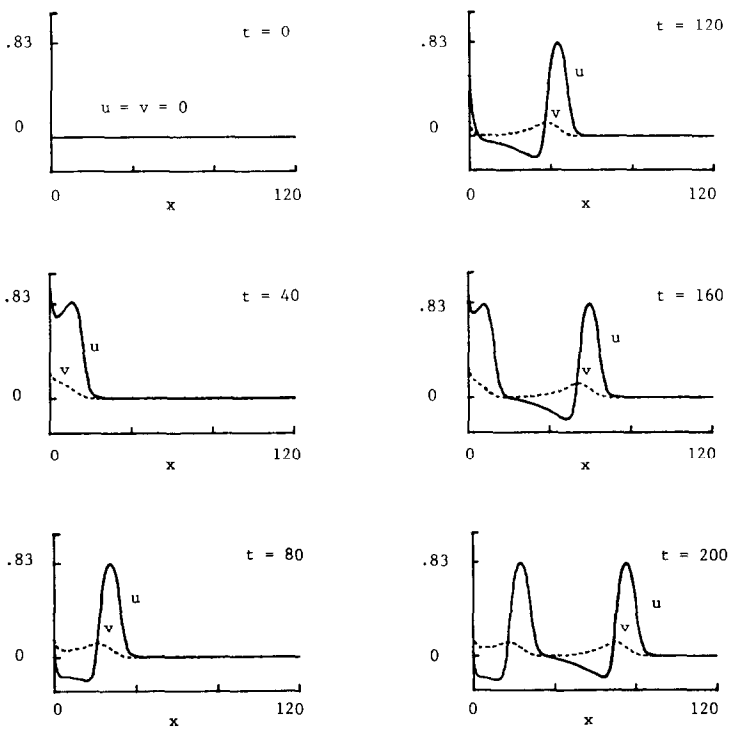

FIG. 6. Solutions of FitzHugh–Nagumo equations in Example 2.

TABLE III

Results for Example 2 (*NONADAPTIVE*): REL ERR $= |||e|||/|||\mathbf{u}|||$ ($\mathbf{u} = \{u, v\}$) and $\Theta = \mathscr{E}/|||e|||$ Computed at $t_p = 20p$, $p = 1,4$

No. elts. (unif.)	ODE TEL	REL ERR mean t_p	REL ERR max t_p	$\lvert\Theta - 1\rvert$ mean t_p	$\lvert\Theta - 1\rvert$ max t_p	CPU
90	$\tau = 10^{-3}$	0.19	0.21	0.09	0.19	8
180	$\tau/2$	0.09	0.10	0.04	0.08	25
360	$\tau/4$	0.05	0.05	—	—	73
720	$\tau/8$	0.02	0.02	—	—	224

was underestimated by 43% when a large (0.2) relative error was requested in the adaptive FEMOL. $\mathscr{E}$ estimated the error much more accurately at the other target times, however, and the quality of $\mathscr{E}$ evidently improves as the relative $|||\cdot|||$-error $\to 0$, in both the adaptive and nonadaptive cases.

By comparing the EPS and max REL ERR entries of Table IV, two failures to achieve error control according to the goal (11) are seen, the failure for EPS $= 0.1$ being "lower level" than that for EPS $= 0.2$. These failures could have been eliminated by "tuning" the algorithm (i.e., allowing regridding to occur before $\mathscr{E}/|||U||| > 0.95$ EPS) or by requesting more accuracy than is actually needed. But these failures show how dependent goal achievement is on the performance of the error estimator in an adaptive method such as the present.

By comparing the NO. ELT. and CPU entries of the last three rows of Tables III and IV, one sees that the mean number of elements used in the adaptive FEMOL was about $\frac{1}{2}$ of the corresponding number of uniform elements, but that the same fraction of CPU time was not saved until the $|||\cdot|||$-error was about 2–3%. This is primarily due to the fact that the traveling fronts in this problem are not very

TABLE IV

Results for Example 2 (*ADAPTIVE*): REL ERR and Θ Computed as in Table III, 80 Uniform Elements Initially, 3-level Macro Grid $\Delta(10, 20, 40)$ Used, REL ERR Estimated and Regridding Permitted at 100 Times in (0, 200]

EPS	MESH MODS	No. elts. mean	No. elts. max	ODE TOL	REL ERR mean t_p	REL ERR max t_p	$\lvert\Theta - i\rvert$ mean t_p	$\lvert\Theta - i\rvert$ max t_p	CPU
$\varepsilon = 0.2$	15	72	80	$\tau = 10^{-3}$	0.22	0.29	0.17	0.43	11
*$\varepsilon/2$	20	82	105	$\tau/2$	0.11	0.13	0.09	0.32	22
$\varepsilon/4$	17	190	221	$\tau/4$	0.04	0.05	—	—	52
$\varepsilon/8$	13	342	442	$\tau/8$	0.02	0.02	—	—	118

localized. As for Example 1, we emphasize that the CPU times for the nonadaptive runs do not reflect the true cost of achieving EPS relative $|||\cdot|||$-accuracy, whereas those for the adaptive runs do.

Note that the number of regriddings remained relatively constant as EPS and TOL $\to 0$ and that the mean number of finite elements appears to have linearly increased with decreasing EPS. These observations are made with almost all of the experiments of this section. They suggest two things:

(1) The regridding strategy is being carried out exactly as planned. Grid shapes are chosen (somewhat stablely) in adapting to the changing nature of the solution, while the numbers of nodes (or grid intensities) are determined by the requested accuracy EPS.

(2) Efficiency demands that pattern reognition notions be used to predict grid shapes, since the number of regriddings will not increase unboundedly as EPS + TOL $\to 0$. The workhorse of the present method is the implicit ODE solver LSODI. The time stepsizes used by LSODI for each space grid decrease as the error tolerances decrease, but the relative distributions (or shapes) of the stepsize sequences change very little. These distributions depend primarily on the shapes of the space grids and higher solution derivatives, and they govern the most appropriate length of time to retain a grid.

The grids constructed in one of the runs for this problem are shown in Fig. 7. The input and results for this run are summarized in the row marked with an asterisk in Table IV. Here, regridding occurred at 20 of the 100 times at which it was allowed. Grid shape selection was guided with the 3-level macro grid $\Delta(10, 20, 40)$, and the parameter EPSDN determining grid intensity was chosen to be no less than 0.8 EPS.

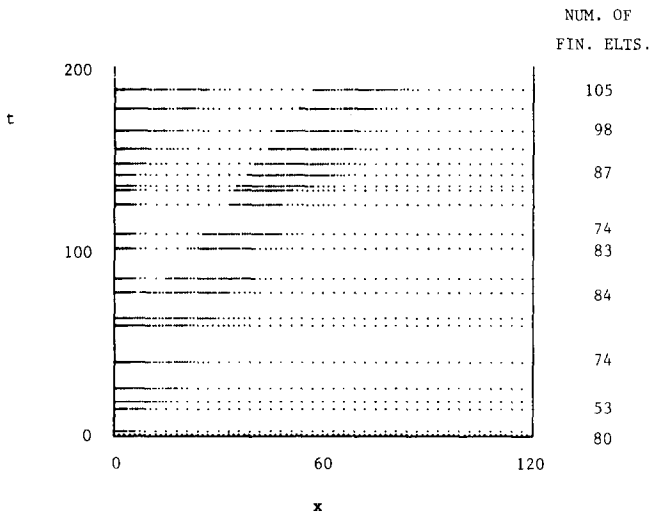

FIG. 7. Adaptively constructed grids for Example 2. Parameters as in * row of Table IV.

Example 3. (Two Counter-Traveling Waves). This model problem was created in order to examine the adaptive FEMOL's performance when two waveforms, having different front widths and directions and speeds of travel, collide and pass through one another. The solution of this problem is

$$u = u^{(1)} + u^{(2)}, \tag{39}$$

where

$$\begin{aligned} u^{(1)}(t, x) &= 0.25(1 + \tanh(100(x - 10t))), \\ u^{(2)}(t, x) &= 0.25(1 + \tanh(80(1 - x - 30t))); \end{aligned} \tag{40}$$

$u^{(1)}$ moves to the right at speed 10 and $u^{(2)}$, whose front width is 25% larger than that of $u^{(1)}$, moves to the left at speed 30. At time $t = 0.025$ the waves collide, almost extinguishing one another. The PDE numerically solved was the scalar heat equation

$$u_t = u_{xx} + f; \qquad t > 0,\ x \in (0, 1), \tag{41}$$

where f, the initial data at $t = 0$, and Dirichlet boundary conditions were set according to (39) and (40).

The results for this problem are summarized in Tables V and VI. The high quality and rapid convergence of the error estimator $\mathscr{E}$ are suggested by the $|\theta - 1|$ columns of both tables. One notes that some of this quality is sacrificed when the grids are nonuniform and allowed to change. The performance of $\mathscr{E}$ here is typical of that we have seen in linear and most mildly nonlinear problems, in which the nonlinearities are polynomial or rational in form.

Error control was achieved in all adaptive runs, with the exception of the low-level failure that occurred with EPS = 0.05. One sees by comparing CPU times in Tables V and VI that the cost in achieving this was only less than that for the uniform, nonadaptive case when the error was about 2–3%. This cost comparison

TABLE V

Results for Example 3 (*NONADAPTIVE*): REL ERR $= |||e|||/|||u|||$ and $\Theta = \mathscr{E}/|||e|||$
Computed at $t_p = 0.01p$, $p = 1,7$

No. elts. (unif.)	ODE TOL	REL ERR mean t_p	REL ERR max t_p	$\lvert\Theta - 1\rvert$ mean t_p	$\lvert\Theta - 1\rvert$ max t_p	CPU
120	$\tau = 10^{-3}$	0.21	0.22	0.031	0.39	8
240	$\tau/2$	0.10	0.11	0.005	0.006	17
480	$\tau/4$	0.05	0.05	0.002	0.002	40
960	$\tau/8$	0.03	0.03	~ 0	~ 0	130

TABLE VI

Results for Example 3 (*ADAPTIVE*): REL ERR and Θ Computed as in Table V, 80 Uniform Elements Initially, 3-Level Macro Grid $\Delta(10, 20, 40)$ Used, REL ERR Estimated and Regridding Permitted at 140 Times in $(0, 0.07]$

		No. elts.			REL ERR		$\lvert\Theta - 1\rvert$		
EPS	MESH MODS	mean	max	ODE TOL	mean t_p	max t_p	mean t_p	max t_p	CPU
$\varepsilon = 0.2$	27	67	83	$\tau = 10^{-3}$	0.18	0.19	0.065	0.154	12
*$\varepsilon/2$	19	105	135	$\tau/2$	0.08	0.09	0.018	0.023	18
$\varepsilon/4$	21	230	287	$\tau/4$	0.04	0.06	0.006	0.009	40
$\varepsilon/8$	25	374	467	$\tau/8$	0.02	0.02	0.002	0.005	115

of course excludes the overhead associated with determining the number of uniform elements needed to obtain a given relative $\|\|\| \cdot \|\|\|$-accuracy EPS.

The grids constructed in one of the adaptive runs are pictured in Fig. 8, along with the locations of the front centers. The input and results for this run are summarized in the row marked with an asterisk in Table VI. One sees that for $0 < t < 0.025$, the regridding frequency was determined automatically by the faster left-moving front, and that nodes were placed ahead of it in an effective manner. For $t > 0.035$ the same was true of the right-moving front.

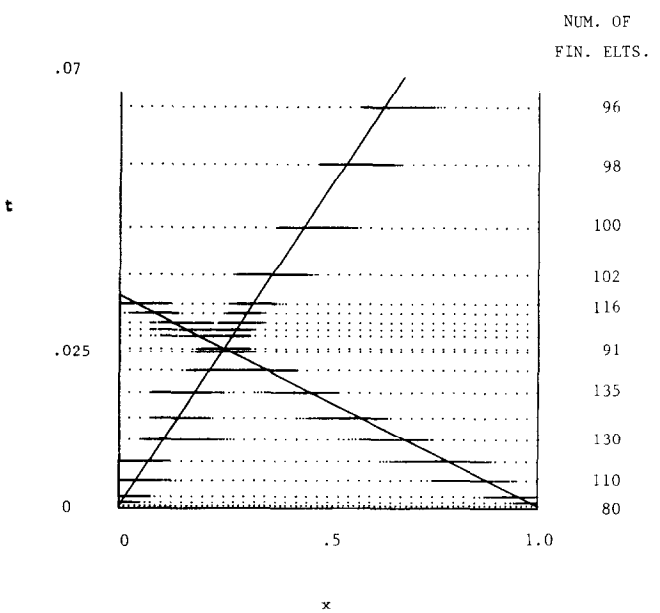

FIG. 8. Adaptively constructed grids for Example 3 and wave centers $x = 10t$ and $x = 1 - 30t$. Parameters as in * row of Table VI.

Example 4. (Dwyer–Sanders Model Flame). This model has been proposed to simulate many of the basic features of flame propagation. It was used as a test problem for the Moving Finite Element method in Gelinas *et al.* [12]. The equations governing a single species mass density ρ and temperature T are

$$\begin{aligned} \rho_t &= \rho_{xx} - f(T)\rho, \\ T_t &= T_{xx} + f(T)\rho, \qquad t > 0,\ x \in (0, 1), \end{aligned} \tag{42}$$

$$\begin{aligned} &\rho_x(t, 0) = \rho_x(t, 1) = 0, \\ &T_x(t, 0) = 0,\ T(t, 1) = g(t),\ t > 0, \end{aligned} \tag{43}$$

and

$$\rho = 1, \qquad T = 0.2, \qquad t = 0,\ x \in (0, 1), \tag{44}$$

where

$$f(T) = 3.52 \times 10^6 \exp(-4/T) \tag{45}$$

and

$$g(t) = \begin{cases} 0.2 + t/(2 \times 10^{-4}), & t \leqslant 2 \times 10^{-4}, \\ 1.2, & t \geqslant 2 \times 10^{-4}. \end{cases} \tag{46}$$

The flame is ignated at $(t, x) = (0, 1)$ and propagates from right to left at a relatively high rate of speed. In the numerical studies here, ρ and T were computed very accurately for $0 \leqslant t \leqslant 2 \times 10^{-4}$, and the values at $t = 2 \times 10^{-4}$ were used as initial conditions for all experimental runs, in which integrations were carried out until time $t = 0.006$.

The steep temperature profiles in the moving temperature–mass density front which were computed in one of the most accurate runs are pictured in Fig. 9. The front propagates at approximately constant speed for $0.003 < t < 0.006$. This

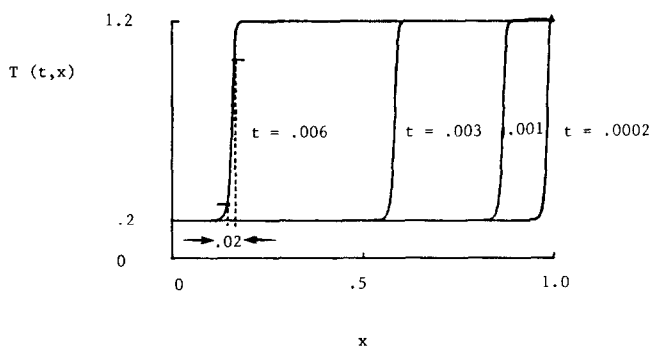

FIG. 9. Temperature T at various times in flame model in Example 4.

TABLE VII

Results for Example 4 (*ADAPTIVE*): REL ERR $= |||e|||/|||\mathbf{u}|||$ ($\mathbf{u} = \{T, \rho\}$) and $\theta = \mathscr{E}/|||e|||$ Computed at $t_p = 5p \times 10^{-4}$, $p = 1,12$; 192 Uniform Elements Initially, 3-Level Macro Grid $\Delta(12, 24, 48)$ Used, ODE TOL $= 2 \times 10^{-6}$ in All Runs, REL ERR Estimated and Regridding Permitted at 290 Times in (0.0002, 0.006]

		No. elts.		REL ERR		$\lvert\Theta - 1\rvert$			
EPS	MESH MODS	mean	max	mean t_p	max t_p	mean t_p	max t_p	CPU	Wave Speed
$\varepsilon = 0.2$	12	62	103	0.55	0.90	0.64	0.86	43	143.6 ± 1.1
$*\varepsilon/2$	22	111	126	0.18	0.35	0.58	0.83	80	142.6 ± 0.3
$\varepsilon/4$	20	170	188	0.05	0.07	0.22	0.43	133	142.23 ± 0.05
$\varepsilon/8$	18	289	353	0.02	0.03	—	—	275	142.11 ± 0.02
$\varepsilon/16$	20	487	724	0.01	0.01	—	—	680	142.08 ± 0.01

problem is much more difficult than the others considered thus far, due to the nature of the nonlinear kinetics. Changing grids to control errors and accurately resolve flame structure is more of a necessity here than a convenience.

The results of applying the adaptive FEMOL to this problem with various requested relative accuracies EPS are summarized in Table VII. The experimental procedure differed from that used in Examples 1–3 in two ways. First, it was not feasible to obtain an almost "exact" solution for comparison by using uniform, non-adaptive finite elements. The first three entries in the REL ERR and $|\theta - 1|$ columns of Table VII were therefore computed by using the approximate solution obtained with the adaptive FEMOL and the parameters in row 5 as "exact." The estimated accuracy of this approximate solution was better at many of the 12 target times than is indicated by the estimated mean and max REL ERR entries in row 5. Second, the same small input ODE error tolerance TOL was used in each run. This was done because the dependence of the time discretization error on TOL was observed to be less smooth in this problem than in the others.

The approximate wave speed for $0.003 < t < 0.006$ in each of the runs is listed in the last column of Table VII. The speeds were computed by monitoring the spatial locations of the $T = 0.5$, 0.75, and 1.0 values on the moving temperature front at 7 evenly spaced times. Those familiar with this model will recognize the accuracies of these speeds, and rapid convergence as EPS $\to 0$ is suggested by the entries.

With the larger input EPS values, the ability of $\mathscr{E}$ to estimate the $|||\cdot|||$-error decays significantly as time increases past 0.003. This can be seen be comparing each of the mean and max $|\theta - 1|$ values in Table VII and would be expected, given the *relatively* inaccurate speeds of propagation. The quality of $\mathscr{E}$ improves as REL ERR $\to 0$, however. This is suggested by the third pair of $|\theta - 1|$ entries and the mass density and temperature gradient profiles computed with various EPS. The temperature gradients computed in many of the runs at the final time are shown in Fig. 10.

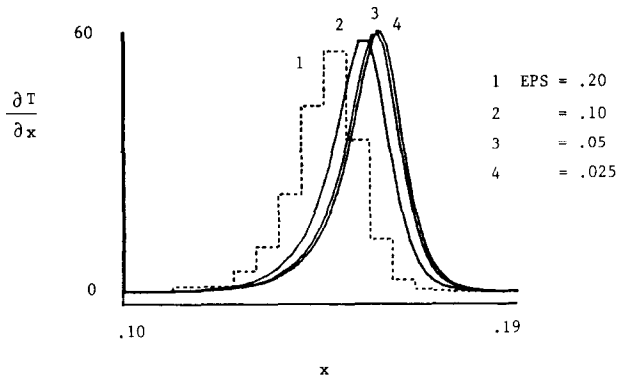

FIG. 10. Temperature gradient at time $t = 0.006$ in Example 4 as computed with various requested relative accuracies.

The ability of the adaptive scheme to control errors according to (11) depends strongly on its ability to estimate the errors. High level failures to achieve (11) are seen in Table VII for large EPS values and the reason for these failures is evident from the similarity of the REL ERR and $|\theta - 1|$ entries. We believe that if failures occurred for the two smallest EPS values, however, then these failures were at a much lower level than those observed for the large EPS values.

To relate the cost of the adaptive FEMOL to that incurred with uniform, nonadaptive elements for this problem, 1000 elements and the same TOL value were used in one nonadaptive run. Over 1200 CPU sec were required to complete the integration. The mean wave speed (as measured before) was 142.19, which along

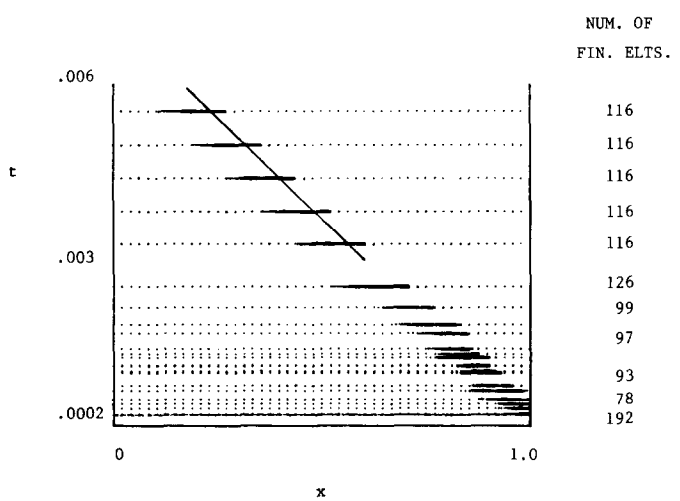

FIG. 11. Adaptively constructed grids for Example 4 and locations of flame center for $0.003 < t < 0.006$. Parameters as in * row of Table VII.

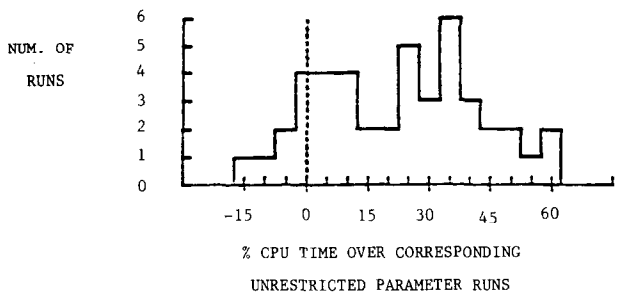

FIG. 12. Added cost in restricting the freedom algorithm in the four examples of this section.

with the observed mass density and temperature gradient profiles indicates that the same accuracy would have been achieved with EPS = 0.04 in the adaptive FEMOL, at less than $\frac{1}{6}$ of the cost.

The automatically constructed grids in one of the runs are shown in Fig. 11, along with the flame center locations for $0.003 < t < 0.006$. The input and results for the run in which these grids were constructed are summarized in the row marked with an asterisk in Table VII. The selection of the space grids was guided with the 3-level macro grid $\Delta(12, 24, 48)$. The construction of the grid at $t = 2.8 \times 10^{-3}$ was

which anticipates the moving front.

We conclude by describing the results of an experiment designed to assess the cost effectiveness of decisions made in adaptive regridding. The most important decisions concern grid shape and intensity. The intensity of a grid is controlled by selecting the parameter EPSDN $\in$ [0.6 EPS, 9 EPS] (cf. Sects. 5, 6). The shape of a grid is controlled by choosing 1 of 3 levels as being "active" on each of the J level 1 macro elements contained in $\Delta(J, 2J, 4J)$ (cf. Sects. 5, 7).

In each of the four examples of this section we restricted the algorithm's freedom to choose these parameters and compared costs with that for an "unrestricted" run. The unrestricted run in each example is that corresponding to the * table entries and that which produced the grids pictured. Eleven restricted runs were made for each problem: EPSDN was fixed as 0.7, 0.8, and 0.9 EPS, the "active" levels in all level 1 macro elements were fixed as the largest and the smallest possible, and all combinations of these EPSDN and "active" level restrictions were imposed.

The CPU times used in the 44 restricted parameter runs were rounded to the nearest multiple of 5% of the corresponding unrestricted run CPU times. These results are summarized by the histogram in Fig. 12. While some of the restricted runs were slightly less expensive, we see that the decisions made by the algorithm are lowering cost the vast majority of the time.

9. Summary

Using piecewise linear finite elements in one space dimension and implicit integration formulas in time, an adaptive method of lines has been developed for a class of nonlinear parabolic partial differential equations. This class includes many equations which are used to model reaction–diffusion phenomena.

The primary goal of this adaptive method is to keep a particular norm of the space discretization error less than a user-specified tolerance EPS at all times. Error control is obtained by adding and deleting space nodes when a computed estimate of the error has nearly exceeded EPS. This process is made efficient, without raising the risk of an error control failure, by monitoring ODE time stepsize information and utilizing multi-grid pattern recognition notions to predict appropriate grid intensities and shapes.

Experiments presented here have shown that the computed error estimates are accurate, that the procedure reliably controls errors, and that the strategy to keep costs low is successful. These experiments were conducted with the program FEMOL 1, which uses the LSODI package to solve the ODE initial value problem resulting from each space grid. Information concerning FEMOL 1 can be obtained by contacting the first author.

The process of collecting information about a solution through local estimates, assimilating this feedback at a more global level, and utilizing features extracted from the global representations was shown here to be an effective and efficient way to automatically construct grids. Many adaptive schemes incorporate this process in one form or another, but the question of how this should best be done has not been adequately addressed.

References

1. I. Babuška and M. Vogelius, "Feedback and Adaptive Finite Element Solution of One-Dimensional Boundary Value Problems," Univ. of Maryland IPST Tech. Note, BN-1006, October 1983.
2. I. Babuška and M. Luskin, *in* "Advances in Computational Methods for Partial Differenctial Equations IV" (R. Vichnevetsky and R. S. Stepleman, Eds.), Vol. 18, p. 5, 1981.
3. I. Babuška and W. Rheinboldt, *Math. Comput.* **33** (1979), 435.
4. M. Berger and J. Oliger, *J. Comput. Phys.* **53** (1984), 484.
5. M. Bieterman, *in* "Adaptive Computational Methods for Partial Differential Equations" (I. Babuška, J. Chandra, and J. E. Flaherty, Eds.), p. 123, SIAM, Philadelphia, Pa., 1983.
6. M. Bieterman and I. Babuška, *Numer. Math.* **40** (1982), 339.
7. M. Bieterman and I. Babuška, *Numer. Math.* **40** (1982), 373.
8. S. F. Davis and J. E. Flaherty, *SIAM J. Sci. Stat. Comput.* **3** (1982), 6.
9. H. A. Dwyer, R. J. Kee, and B. R. Sanders, *AIAA J.* **18** (1980), 1205.
10. J. E. Flaherty, J. M. Coyle, R. Ludwig, and S. F. Davis, *in* "Adaptive Computational Methods for Partial Differential Equations" (I. Babuška, J. Chandra, and J. E. Flaherty, Eds.), p. 144, SIAM, Philadelphia, Pa., 1983.
11. D. Gannon, "Self-adaptive Methods for Parabolic Partial Differential Equations," Ph. D. thesis, University of Illinois, Urbana–Champaign, 1980.

12. R. J. GELINAS, S. K. DOSS, AND K. MILLER, *J. Comput. Phys.* **40** (1981), 202.
13. A. HARTEN AND J. M. HYMAN, *J. Comput. Phys.* **50** (1983), 235.
14. A. C. HINDMARSH, "Toward a Systemized Collection of ODE Solvers," Report UCRL-874645, Lawrence Livermore National Laboratory, Livermore, California, 1983.
15. A. C. HINDMARSH, "LSODE and LSODI, Two New Initial Value Ordinary Differential Equation Solvers," ACM SIGNUM Newsletter, Vol. 15, p. 10, 1980.
16. K. MILLER AND R. MILLER, *SIAM J. Numer. Anal.* **18** (1981), 1019.
17. K. MILLER, *SIAM J. Numer. Anal.* **18** (1981), 1033.
18. A. R. MITCHELL AND V. S. MANORANJAN, *in* "Mathematics of Finite Elements and Applications IV" (J. R. Whiteman, Ed.), p. 17, Academic Press, New York, 1982.
19. J. D. MURRAY, "Lectures on Nonlinear–Differential–Equation Models in Biology," Oxford Univ. Press, Oxford, 1977.
20. W. RHEINBOLDT, *in* "Adaptive Computational Methods for Partial Differential Equations" (I. Babuška, J. Chandra, and J. E. Flaherty, Eds.), p. 3, SIAM, Philadelphia, Pa., 1983.
21. J. RINZEL, *in* "Nonlinear Diffusion; Research Notes in Mathematics 14" (W. E. Fitzgibbon (III) and H. F. Walker, Eds.), p. 186, Pitman, London, 1977.
22. J. F. THOMPSON, Z. U. A. WARSI, AND C. W. MASTIN, *J. Comput. Phys.* **47** (1982), 1.